Journal of Power Sources 253 (2014) 214–223

Contents lists available at ScienceDirect

Journal of Power Sources

journal homepage: www.elsevier.com/locate/jpowsour

Facile synthesis of morphology-controlled Co_3O_4 nanostructures through solvothermal method with enhanced catalytic activity for H_2O_2 electroreduction

Kui Cheng, Dianxue Cao, Fan Yang, Yang Xu, Gaohui Sun, Ke Ye, Jinling Yin, Guiling Wang*

Key Laboratory of Superlight Material and Surface Technology of Ministry of Education, College of Material Science and Chemical Engineering, Harbin Engineering University, Harbin 150001, China

HIGHLIGHT

- Co_3O_4 with different morphologies are synthesized *via* a simple solvothermal method.
- The influences of solvent and probable growth mechanism are discussed.
- The electrode exhibits high performance and good stability for H_2O_2 reduction.

GRAPHICAL ABSTRACT

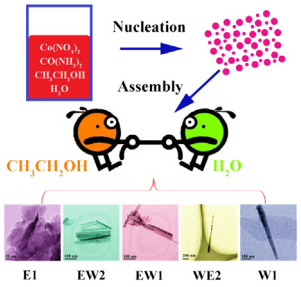

ARTICLE INFO

Article history:
Received 30 August 2013
Received in revised form
14 November 2013
Accepted 14 December 2013
Available online 24 December 2013

Keywords:
Solvothermal
Morphology-controlled
Cobalt oxide
Nanostructure
Hydrogen peroxide electroreduction

ABSTRACT

Hydrogen peroxide (H_2O_2) replaced oxygen (O_2) as oxidant has been widely investigated due to its faster reduction kinetics, easier storage and handling than gaseous oxygen. The main challenge of using H_2O_2 as oxidant is the chemical decomposition. In this article, by using different C_2H_5OH/H_2O volume ratio as the solvent, Co_3O_4 with different morphologies (nanosheet, nanowire, ultrafine nanowire net, nanobelts, and honeycomb-like) direct growth on Ni foam are synthesized *via* a simple solvothermal method for the first time. Results show that the introduction of ethanol could obviously improve the catalytic performance toward H_2O_2 electroreduction. The sample prepared in the solution with the C_2H_5OH/H_2O volume ratio of 1:2 shows the best catalytic performance among the five samples and a current density of 0.214 A cm^{-2} is observed in 3.0 mol L^{-1} KOH + 0.5 mol L^{-1} H_2O_2 at −0.4 V (*vs.* Ag/AgCl KCl), which is much larger than that on the other metal oxides reported previously, almost comparable with the precious metals. This electrode of Co_3O_4 directly grown on Ni foam has superior mass transport property, which combining with its low-cost and facile preparation, make it a promising electrode for fuel cell using H_2O_2 as the oxidant.

1. Introduction

Recently, due to its faster reduction kinetics, easier storage and handling than gaseous oxygen, hydrogen peroxide (H_2O_2) replaced oxygen (O_2) as oxidant has been widely investigated in several types of low-temperature fuel cell, such as direct methanol-hydrogen peroxide fuel cell (DMPFC) [1,2], direct hydrogen peroxide-hydrogen peroxide fuel cell (DPPFC) [3,4], direct borohydride-hydrogen peroxide fuel cell [5,6], and metal-hydrogen peroxide fuel cell [7,8]. However, the main issue of using H_2O_2 as oxidant is the chemical decomposition result in the formation of O_2 bubbles, which not only reduces the utilization efficiency of H_2O_2

* Corresponding author. Tel./fax: +86 451 82589036.
E-mail address: wangguiling@hrbeu.edu.cn (G. Wang).

0378-7753/$ – see front matter © 2013 Elsevier B.V. All rights reserved.
http://dx.doi.org/10.1016/j.jpowsour.2013.12.068

but also increases the difficulty of the battery design. Nowadays, nano-materials have attracted much attention due to their unique physical and chemistry properties [9–13]. Therefore, studies on the controlled fabrication of nanostructures such as nanoparticles [14], nanowires [15], and nanosheets [16] with functional properties have been widely developed in recent years. The unique properties of nano-materials in facilitating the mass transport, ion diffusion and electron transfer, thus dramatically boosting the electrochemical performance [17,18], suggests that the main challenge of using H_2O_2 as oxidant could be resolved or greatly ameliorated.

Co_3O_4 is an important material for electrochemical energy storage, sensors, and catalysis [19–25]. For example, Co_3O_4 exhibited promising activity and stability for catalytic electroreduction of H_2O_2 in alkaline medium [19]. Besides, Co_3O_4 is also particularly attractive for application in electrochemical capacitors, due to its low cost, low environmental footprint, great redox activity and extremely high theoretical specific capacitance (*ca.* 3560 F g^{-1}) [20]. Co_3O_4 has also been reported as the high-performance anode in the lithium batteries [25]. Currently, tremendous efforts have been devoted to the rational synthesis of Co_3O_4 nanostructure direct growth on substrate. In general, self-supported nano-materials growing directly on a current-collecting substrate represent an amazing architecture. Such structures have been demonstrated to usually possess larger electrochemical active surface area, higher utilization efficiency of the active materials, and superior mass transport property than conventional electrodes fabricated by mixing and pressing powder of active material with conducting materials (e.g., carbon black) and polymer binders (e.g., polytetrafluorethylene) [26–29]. Li and co-workers [30] investigated the performance of Pt and Pt–Ru nanowire array electrodes obtained *via* an anodic aluminum oxide (AAO) template on a Ti/Si substrate as the anode of direct methanol fuel cell and found that these electrodes have a high electrode area and the surface of the metals is nearly one hundred percent used in contrast to the traditional gas diffusion electrode, in which the utilization of the surface of the catalysts is usually less than 85% due to the addition of carbon and polymer binder. Our recent study [19] also demonstrates that Co_3O_4 nanowire arrays directly grown on Ni foam exhibited higher activity and stability for catalytic electroreduction of H_2O_2 in alkaline medium than Co_3O_4 nanoparticles. State of the art, Solid template and structure-directing agents are commonly used to fabricate materials with hierarchical structures [31–33]. However, some problems and challenges still remain, since that complete template removal is needed, which means a much more complicated process including the selection of appropriate solvent or calcination at elevated temperature. Furthermore, impurities can be introduced from the templates or agents that affect the properties adversely. Compared with these methods, hydrothermal/solvothermal synthesis is an effective method to prepare novel materials under mild temperature and high pressure in sealed apparatus. Diverse products with different composition, structure and morphology can be achieved by simply adjusting the hydro(solvo)-thermal conditions (including solution pH, the addition of extra reactants, the temperature and the time of the process). More importantly, the whole process is economic, facile and environmentally friendly [34–36]. Zhu et al. [37] prepared Co_3O_4 flowers by thermal decomposition of $Co(OH)_2$ which are obtained by the hydrolysis of cobalt acetate in solvent mixtures containing the polyalcohol and deionized water. Yu et al. [38] also synthesized uniform Co_3O_4 crystals with different shapes through tuning the volume ratio of a mixed solvent composed of water and ethanol (or glycerol). Wang's group [39] designed a facile and versatile water-controlled precipitation approach for preparation of various Co_3O_4 nanostructures, including nanorods, nanowires, and layered parallel folding nanostructures. Zhao and co-author [40] illustrate the successful synthesis of tetragonal dipyramid Co_3O_4 powders *via* a versatile non-aqueous reaction system using benzyl alcohol solvent.

To our knowledge, the preparation of Co_3O_4 nano-materials direct growth on substrate with different morphologies through solvothermal synthesis has rarely been reported. Hereby, we report the morphology-controlled synthesis of Co_3O_4 nanostructure (nanowires, nanosheets, nanobelts, nano-honeycomb and ultrafine nanowires net) supported on Ni foam substrate *via* a solvothermal treatment in the mixed water–ethanol solvent system. We used solutions with different ratios of ethanol to water and investigated the effects of the ethanol fraction in solution. The changes in the size, morphology and composition of the product as a function of the water/ethanol fraction were examined. The possible growth mechanism was also discussed. In addition, the catalytic activity of these Co_3O_4 nanostructures for H_2O_2 electroreduction in alkaline medium has been also systematically investigated. Result showed the introduction of ethanol could obviously improve the catalytic performance toward H_2O_2 electroreduction.

2. Experimental

2.1. Preparation of Co_3O_4 nano-materials with different morphologies supported on Ni foam substrate

Ni foam supported Co_3O_4 nano-materials were prepared *via* a solvothermal synthesis, followed by a calcination process in air. The Ni foam (23 × 40 × 1.1 mm^3, 110 PPI, 320 g m^{-2}; Changsha Lyrun Material Co., Ltd. China) was pretreated by degreasing with acetone, etching with 6.0 mol dm^{-3} HCl for 15 min, rinsing with water and prior to use. In a typical synthesis, a 24 mL solution consisting of 4 mmol $Co(NO_3)_2$, 10 mmol $CO(NH_2)_2$ and C_2H_5OH/H_2O mixtures in volume ratio of 1:0, 2:1, 1:1, 1:2 and 0:1 was first stirred for 15 min in air at the room temperature. The obtained homogeneous solution was then transferred into a 30 mL Teflon-lined stainless steel autoclave. A piece of Ni foam was then put into the autoclave and immersed in the solution. The autoclave was maintained at 90 °C for 10 h to allow the precursor with different morphologies growth on Ni foam. After that, the autoclave was cooled down to room temperature and the Ni foam was removed from the growth solution, thoroughly washed with water, dried at 60 °C, and finally calcined at 300 °C for 3 h in air.

2.2. Characterization of Co_3O_4 nano-materials

The as-prepared samples morphology was characterized by a scanning electron microscope (SEM, JEOL JSM-6480) and a transmission electron microscope (TEM, FEI Teccai G2S-Twin, Philips). The structure was analyzed using an X-ray diffractometer (Rigaku TTR III) with Cu Kα radiation ($\lambda = 0.1514178$ nm). Chemical bonding information on metal-oxygen and carbonate were investigated with Fourier transform infrared spectroscopy (FTIR, Equinos 55, Bruker) using the potassium bromide pellet technique. Each FTIR spectrum was collected after 16 scans with a resolution of 0.5 cm^{-1}. Thermogravimetric (TG) was performed with a Pyris-Diamond thermal analyzer (Perkin–Elmer) in a flow of air (40 cm^3 min^{-1}) at a heating rate of 20 °C min^{-1} from room temperature up to 600 °C in an Al_2O_3 sample pan.

2.3. Electrochemical measurements

The as-prepared Co_3O_4 performance of the H_2O_2 electrochemical reduction was measured by linear scan voltammetry (LSV) and chronoamperometry (CA) in a standard three-electrode electrochemical cell with an Ag/AgCl, KCl electrode reference

electrode and a Pt foil counter electrode using KOH as the electrolyte at the room temperature (25 ± 1 °C). The reported current densities were calculated using the geometrical area of the electrode (1 cm^2). All solutions were made with analytical grade chemical reagents and ultra-pure water (Milli-Q 18 MΩ cm). All potentials were referred to the saturated Ag/AgCl, KCl electrode reference electrode. All measurements were performed at room temperature and all the electrolytes were deoxygenated by N_2 bubbling.

3. Results and discussion

3.1. Characterization of the as-prepared samples prepared with different C_2H_5OH/H_2O volume ratios

Fig. 1 shows the optical image of the growth solution with different volume ratios of C_2H_5OH/H_2O mixtures and the Ni foam-supporting Co_3O_4 nano-materials at different preparation stages. As we know, the Co^{2+} exists in the form of $[Co(H_2O)_6]^{2+}$ in an aqueous solution. H_2O molecules of $[Co(H_2O)_6]^{2+}$ will be partly replaced by ethanol molecules when introduced ethanol in the solution mixtures, resulting in the transformation of cobalt complex into $[Co(H_2O)_a(CH_3CH_2OH)_{6-a}]^{2+}$. So the color of reaction solutions turns into darker along with the increase of ethanol volume. The Ni foam was first cut into a 23 × 40 mm^2 sheet, cleaned, polished (Fig. 1a) and then put into the Teflon reactor. After solvothermal treatment in the mixed water–ethanol solvent, the surface of Ni foam substrate was uniformly covered by a layer of products with a gradually changing color (deep pink-claybank-light pink). After calcination, the products with various color turned to a black color (Fig. 1g). And the samples prepared using different C_2H_5OH/H_2O volume ratios of 1:0, 2:1, 1:1, 1:2 and 0:1 were denoted as E1, EW2, EW1, WE2 and W1, respectively.

The decomposition TG curves of the precursor (Fig. 2) are shown that the thermal process proceeds *via* three stages under an air atmosphere. The weight loss and the stage temperature were listed in Table 1. At the first stage, the weight loss can be attributed to the evaporation of water physically adsorbed on the surface, trapped in intercrystalline pores, and intercalated in the interlayer space [41]. The second stage might correspond to the decomposition of precursor [42,43]. The last weight loss can be ascribed to the further decomposition of precursor and crystallization of Co_3O_4. It can also reveal that the temperature of stage II increased as the C_2H_5OH/H_2O volume ratio decreased. Thus it can be inferred that the C_2H_5OH/H_2O volume ratio influences the composition of the precursor.

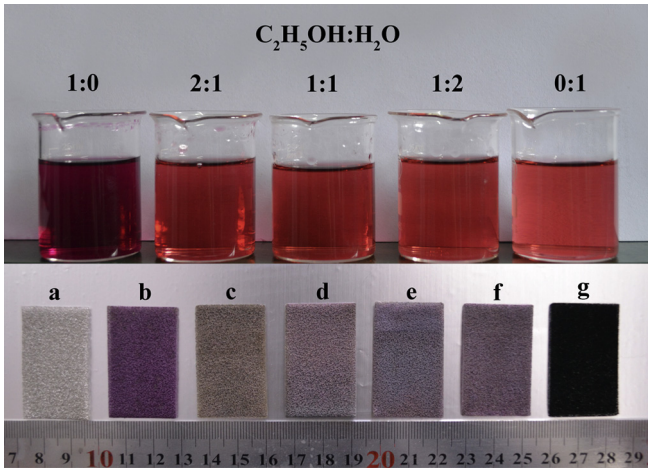

Fig. 1. Photographs of the growth solution with different volume ratio of C_2H_5OH/H_2O mixtures; Ni foam (a), the corresponding precursor of different morphologies of Co_3O_4 nano-structures on Ni foam (b–f) and Co_3O_4/Ni foam after calcinations (g).

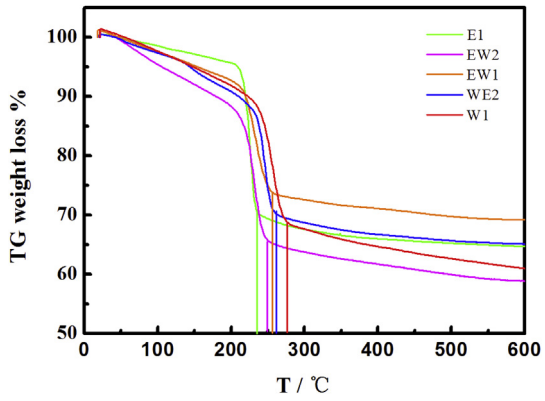

Fig. 2. Thermogravimetric profiles of as-prepared precursors in the growth solution with different C_2H_5OH/H_2O volume ratios (E1, EW2, EW1, WE2 and W1).

Fig. 3 shows the XRD patterns of as-prepared Co_3O_4 in the growth solution with different C_2H_5OH/H_2O volume ratio (E1, EW2, EW1, WE2 and W1) before (a) and after (b) annealing, respectively, and the standard date of spinel-phased Co_3O_4 crystal (JCPDS NO. 43-1003). As shown, all the samples before the annealing are different and weak crystal. Taken the sample E1 as an example, the peak appeared at 12.8° could be assigned to $Co(OOCCH_3)_2 \cdot 4H_2O$ (JCPDS NO. 29-0465), indicating that ethanol is oxidated in the solvothermal process, and further reacts with Co^{2+}. The peak of W1 could be due to the $Co(CO_3)_{0.5}(OH)0.11H_2O$ (JCPDS NO. 48-0083). For the as-prepared samples with different C_2H_5OH/H_2O volume ratios (EW2, EW1 and WE2), the precursors are actually the mixtures of $Co(OOCCH_3)_2 \cdot 4H_2O$ and $xCoCO_3 \cdot yCo(OH)_2 \cdot zH_2O$. Based on the above TG results, we subsequently treat this as-synthesized product at 300 °C for 3 h in air. Although the temperature is not high enough for the total decomposition of precursors, however, the main phase of the samples is spinel Co_3O_4 phase after annealing, indicating that the rest of precursor is quite a few and the crystal planes for each peak is marked. Moreover, it can also be seen from Fig. 3 that the different C_2H_5OH/H_2O volume ratios just influence the composition of crystal phase in the precursors, and all the different precursors can finally turn into the spinel Co_3O_4 phase after annealing.

The FTIR spectra of the as-prepared samples are presented in Fig. 4. Two wide bands were registered for Co_3O_4 sample, one in the region 550–575 cm^{-1} ($\lambda 1$) and another in the interval 650–675 cm^{-1} ($\lambda 2$). In general, the first one is attributed to the stretching vibration of Co^{3+}–O bond, where Co^{3+} is in an octahedral position and the second one is the stretching vibration of Co^{2+}–O bond (Co^{2+} in a tetrahedral position) [44]. Compared with the sample

Table 1
The weight loss and the stage temperature of the precursor.

Sample	Stage I	Stage II	Stage III
E1	0–206 °C	207–235 °C	236–600 °C
	4.5% loss	25% loss	5.8% loss
EW2	0–200 °C	201–250 °C	251–600 °C
	11.6% loss	22.6% loss	7.0% loss
EW1	0–210 °C	211–260 °C	261–600 °C
	7.1% loss	19.3% loss	4.4% loss
WE2	0–222 °C	223–262 °C	263–600 °C
	11.2% loss	18.6% loss	5.1% loss
W1	0–230 °C	231–−277 °C	278–600 °C
	10.7% loss	20.6% loss	7.7% loss

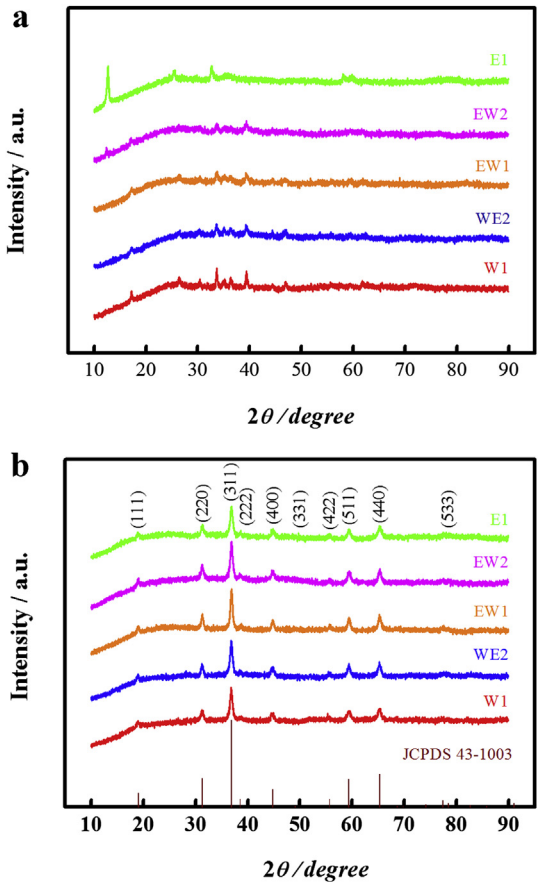

Fig. 3. XRD patterns of as-prepared Co_3O_4 nanostructures in the growth solution with different C_2H_5OH/H_2O volume ratios (E1, EW2, EW1, WE2 and W1) before (a) and after (b) annealing at 300 °C for 3 h in air, respectively.

W1, these peaks in the other four samples obtained from the solution containing ethanol shifted to high wave number, suggesting a decrease in the strength of Co–O bond in Co_3O_4.

In order to further study the reaction mechanism, the growth solutions of E1 before and after solvothermal reaction were also investigated by FTIR (Fig. 5). As it shown, the broad band at around 3500–3300 cm^{-1} before solvothermal reaction splits into two peaks, which can be ascribed to the vibration of –OH and –NH form CH_3CH_2OH and $CO(NH_2)_2$ [45–47]. As for the solution before solvothermal reaction, there are three small bands at 2980, 2792 and 2729 cm^{-1} originated from the asymmetric and symmetric

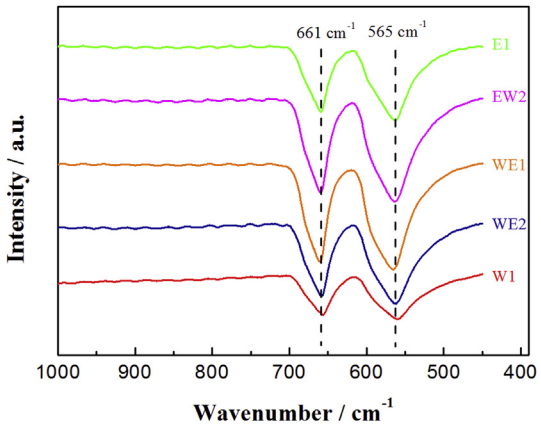

Fig. 4. FT-IR spectra of as-prepared Co_3O_4 nanostructures in the growth solution with different C_2H_5OH/H_2O volume ratios.

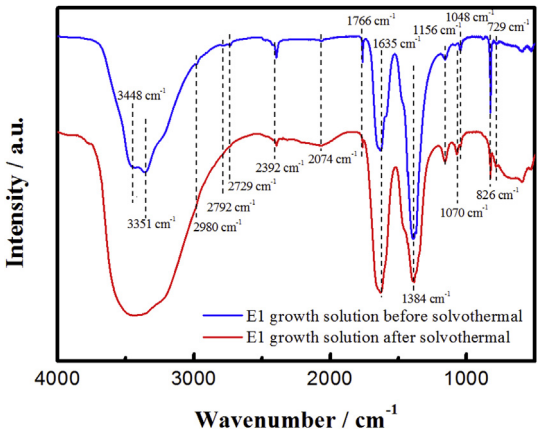

Fig. 5. FT-IR spectra of the E1 growth solution before and after solvothermal reaction.

stretching bands of $-CH_2-$ and $-CH_3-$, however, not obvious in the solution after reaction [45,46]. The peaks at 1708 and 1457 cm^{-1} is due to the mode of the $-NO_3$ stretching vibration [48]. The evidence for the presence of CO_3^{2-} is confirmed by its fingerprint peaks of D_{3h} symmetry at 1070 and 729 cm^{-1}. The band shown at 2476 cm^{-1} is also ascribed to vibrational mode of the carbonate anions [49,50]. The 1635 and 1384 cm^{-1} bands appeared in both before and after solvothermal growth solution are characteristic of stretching vibration of the –C=O and –N–C=O, respectively [47,51–53]. However, after the solvothermal reaction, the relative strength of –C=O increases, implying that the amount of –COOH increases in the growth solution after reaction. Based on the analysis of the XRD, the FTIR on the growth solution can also demonstrate that, besides acting as solution, the ethanol also takes part in the reaction of the Co_3O_4 product.

The Co_3O_4 nano-materials synthesized in the growth solution with different C_2H_5OH/H_2O volume ratios have rather different morphologies, as shown in Fig. 6. It can be seen that all the five samples exhibit relatively uniform, well-dispersed morphology within submicron size range, yet the specific sizes and morphologies of the samples prepared with different solvents are very different. And after oxidative conversion into Co_3O_4, the basic morphology of the sample is perfectly conserved without calcination-induced significant alterations. The Co_3O_4 grown from the ethanol solvent without water (Fig. 6A and B) exhibited a nanosheet micro-structure with the thickness of 100–200 nm. The nanosheets interconnected with each other, which created loose porous nano-structures with abundant open space and electroactive surface sites. When the mixture of C_2H_5OH/H_2O with the volume ratio 2:1 was used as the solvent, the SEM image of as-prepared nano-structure displayed the belt-like morphology. According to Fig. 6C and D, nanobelts attached to each other closely and distributed on the surface of Ni foam. Further increasing the water volume ratio of the solvent (1:1), a honeycomb-like Co_3O_4 nanostructure uniformly covered the surface of Ni foam (Fig. 6E and F). For the sample prepared in the solvent with the volume ratio C_2H_5OH/H_2O of 1:2, an ultra-fine nanowire net (Fig. 6G and H) was obtained. For the sample prepared in pure deionized water, a nanowire array was grown on the Ni foam (Fig. 6I and J). It is worth to note that all the morphologies were assembled by several nanowires with the solvent containing water. TEM and HRTEM images of the as-prepared Co_3O_4 samples before and after calcined are displayed in Fig. 7, providing an insight of different structures. It can be obtained that calcination resulted in obvious changes in the morphology of an individual nanowire, but the overall array structure was still maintained. After calcinations, the solid nanostructure was converted to porous structure, which is composed of

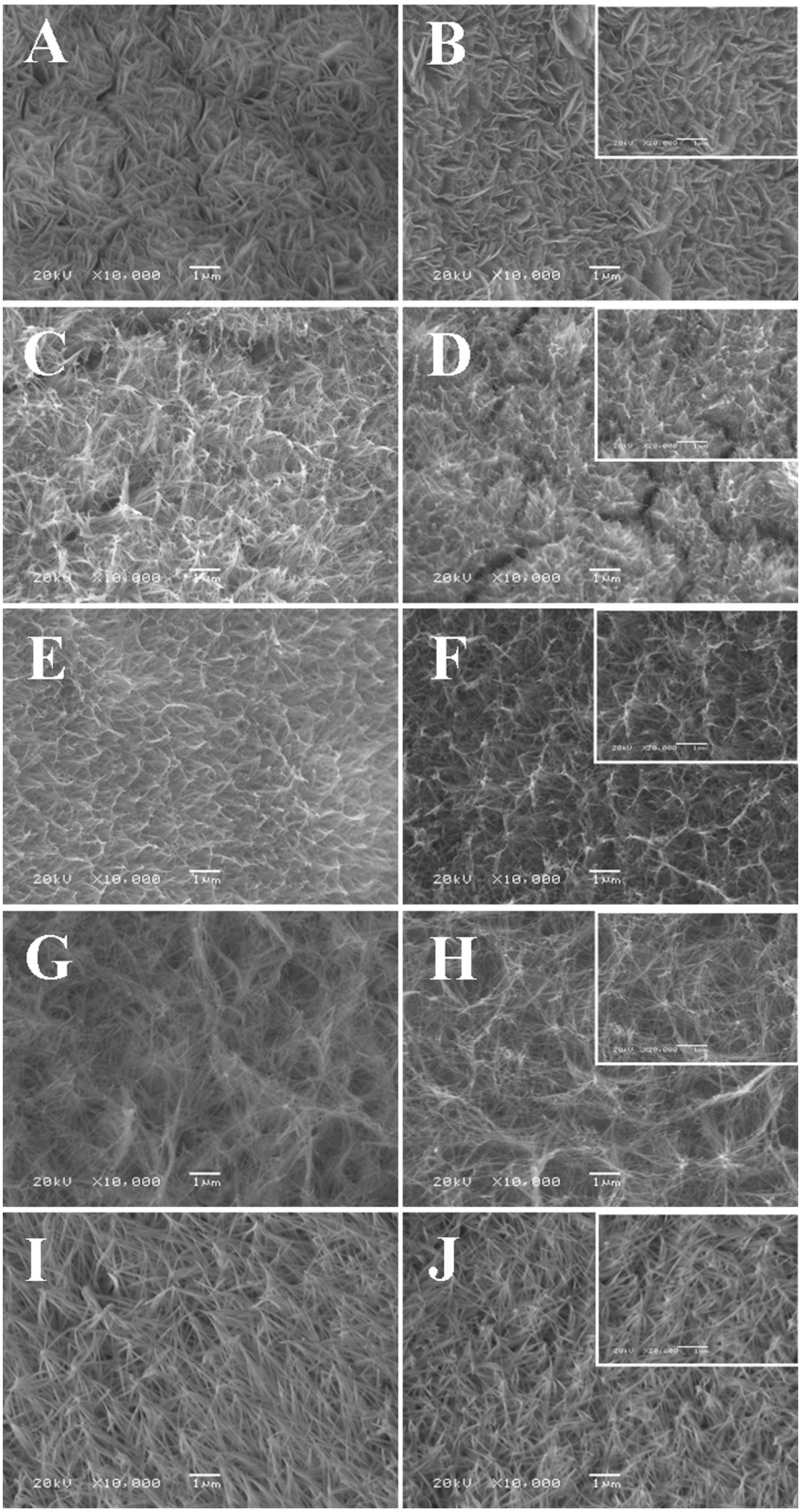

Fig. 6. SEM images of as-prepared Co_3O_4 nanostructures in the growth solution with different C_2H_5OH/H_2O volume ratios: E1 before (A) and after (B) calcined, EW2 before (C) and after (D) calcined, EW1 before (E) and after (F) calcined, WE2 before (G) and after (H) calcined and W1 before (I) and after (J) calcined. Inset is the high-magnified SEM images of the as-prepared samples.

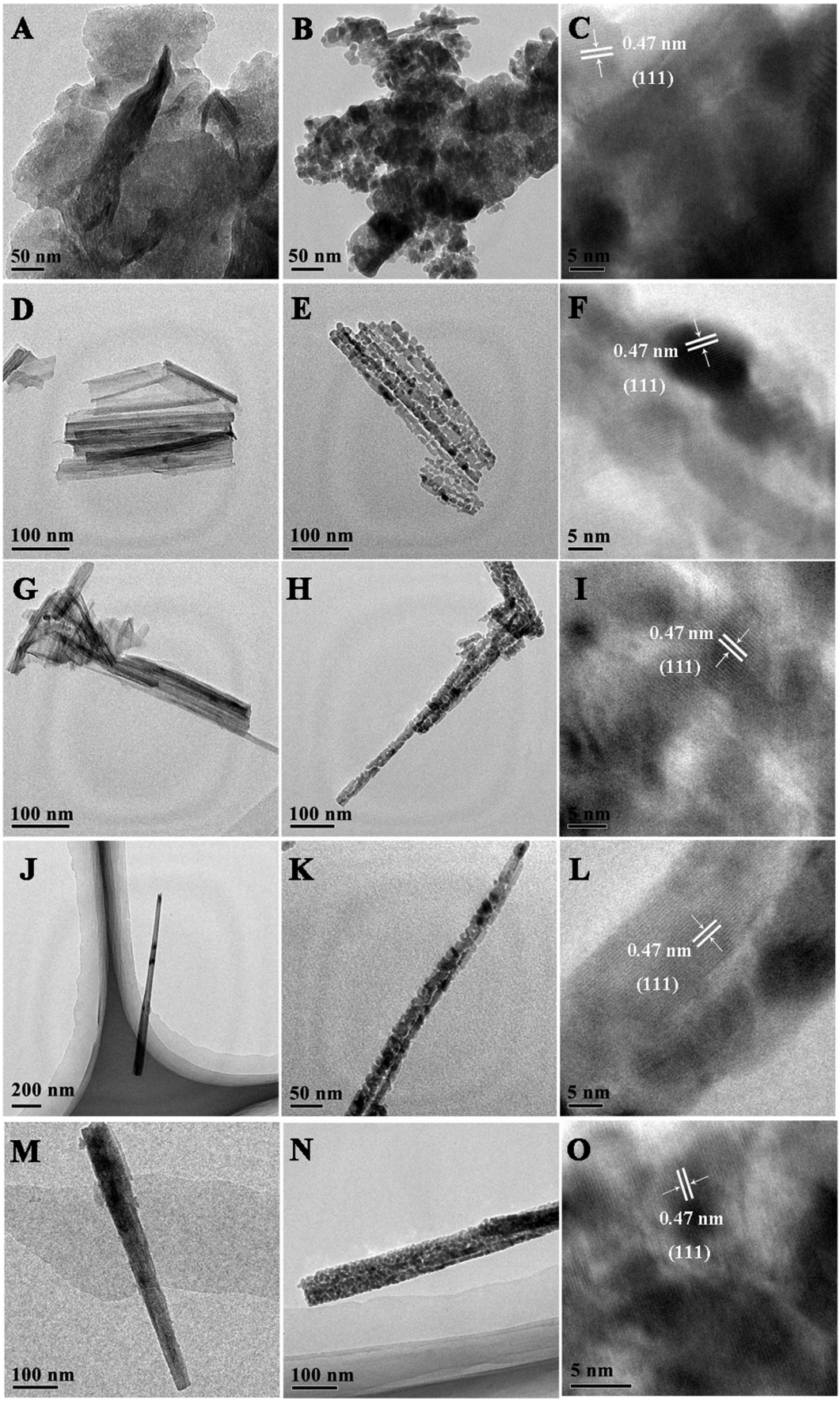

Fig. 7. TEM and HRTEM images of as-prepared Co_3O_4 nanostructures in the growth solution with different C_2H_5OH/H_2O volume ratios: E1 before (A) and after (B) calcined and HRTEM images (C), EW2 before (D) and after (E) calcined and HRTEM images (F), EW1 before (G) and after (H) calcined and HRTEM images (I), WE2 before (J) and after (K) calcined and HRTEM images (L) and W1 before (M) and after (N) calcined and HRTEM images (O).

interconnected nanoparticles. TEM images of the sample E1 (Fig. 7A and B) confirm its assembly as a sheet-like structure. Unlike sample E1, the belt-like structure of sample EW2 is assembled by several nanowires and the diameter is about 100 nm. For the sample EW1, we can see that the sample has a T-end structure, which is composed of a nanowire in the bottom and a sheet in the top. For the sample WE2 and W1, they were all the nanowire-like, but the diameter of WE2 is much thin than that of W1. High-resolution TEM (HRTEM) images of the head in Fig. 7C, F, I, L and O demonstrate the clear lattice fringes and the distance (0.47 nm) agrees well with the (111) crystal plane of Co_3O_4 (JCPDS NO. 43-1003, $d_{111} = 0.47$ nm). That also confirmed that the as-prepared samples growth in different solvent were pure spinel Co_3O_4 phase.

3.2. Growth mechanism

Based on the above analysis, Co_3O_4 nano-size crystals with different morphologies can be obtained through a simple solvothermal method. Generally speaking, during the synthesis process, the solvent influences the size and structure of the final products, as demonstrated in Scheme 1. At first, numerous tiny precursor crystalline nuclei appear on the Ni foam and then the crystal growth follows. The major reactions occurred at this stage in aqueous solution are most investigated as following [54,55]:

$$CO(NH_2)_2 + 4H_2O \rightarrow H_2CO_3 + 2NH_3 \cdot H_2O \quad (1)$$

$$NH_3 \cdot H_2O \rightarrow NH_4^+ + OH^- \quad (2)$$

$$H_2CO_3 \rightarrow 2H^+ + CO_3^{2-} \quad (3)$$

$$(x+y)Co^{2+} + yCO_3^{2-} + xOH^- + zH_2O \rightarrow xCo(OH)_2 \cdot yCoCO_3 \cdot zH_2O \quad (4)$$

However, when the ethanol was used as solvent, on the basis of the result above (TG, XRD and FTIR), there are another reaction happened:

$$CH_3CH_2OH + O_2 \rightarrow CH_3COOH + H_2O \quad (5)$$

$$2CH_3COOH + Co^{2+} \rightarrow (CH_3COO)_2Co + 2H^+ \quad (6)$$

So the precursor is a mixture of $(CH_3COO)_2Co$ and $xCoCO_3 \cdot yCo(OH)_2 \cdot zH_2O$, and the solvent ratio directly influences the composition of precursor. With the reaction proceeding, these tiny nuclei gradually grow larger. The different nanostructures of Co_3O_4 were mainly determined by this stage. Since solvent ratio is the only difference during the synthesis, it should be the key factor for the different sizes and morphologies. As we know, the polarity between water and ethanol is different. So, the polarity of solvents influences not only the nucleation of the precursor but also the preferential direction of crystal growth. Ayudhya [56] reported that solvents with lower polarity helped to cultivate rods with high aspect ratios for ZnO prepared in a solvothermal conditions. Our findings on the effects of solvent polarity are similar to that reported. With the H_2O volume increased, the morphology tends to rod-like, on the contrary, the morphology turns into flake-like. The competition effect between ethanol and water relation leads to the obvious change in the morphology and size. In a word, the growth solution containing different ethanol/water ratios is the fundamental reason of the formation of Co_3O_4 with different nanos-

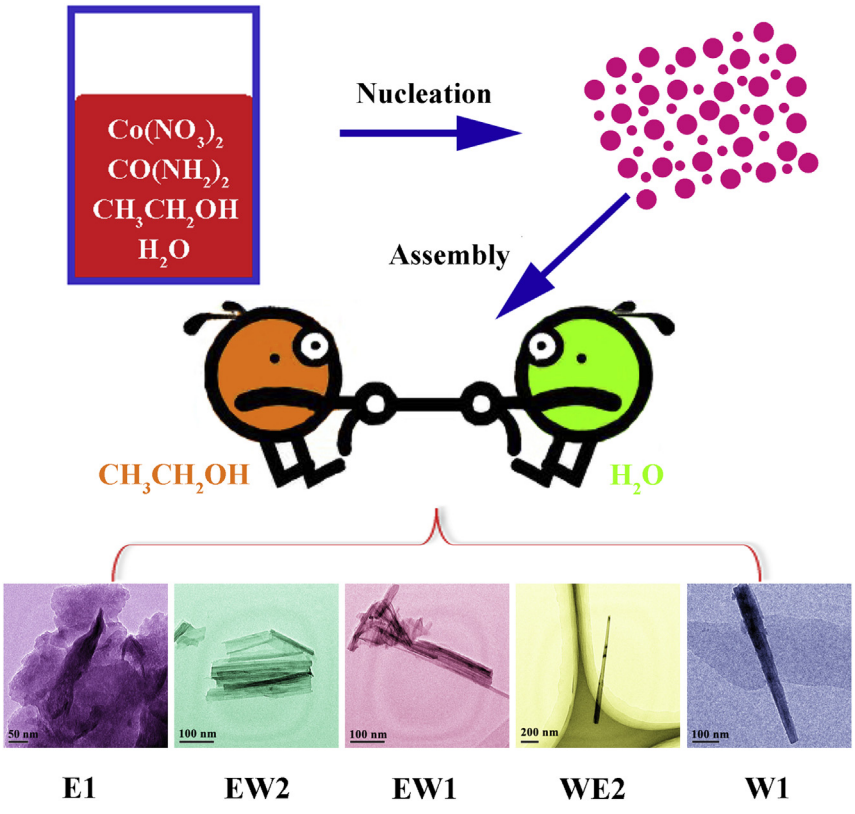

Scheme 1. Schematic diagram showing the mechanism for the formation of different nanostructures Co_3O_4.

tructure. By the way, other factors in the preparation process, such as vapor pressure and solubility of the precursors in the solvent, need further studies.

3.3. Electrocatalytic performance of H_2O_2 electroreduction on the samples prepared in the solvent with different C_2H_5OH/H_2O volume ratios

Fig. 8 shows the cyclic voltammograms (CV) of the different Co_3O_4 samples prepared with the solvent containing different C_2H_5OH/H_2O volume ratios in 3.0 mol L^{-1} KOH. The CV of pristine Ni foam is also shown for comparison. It can been seen that Ni foam only showed a pair of redox peaks which is corresponding to the interconversion between Ni(II) and Ni(III) (Eq. (7)) [57]. CV measurement of the as-prepared samples displayed the characteristic response of Co_3O_4 in an alkaline solution. The anodic peaks were caused by the conversion of Co(II)/Co(III) (Eq. (8)) and further oxidated to Co (IV) (Eq. (9)). In the reverse sweep, the cathodic peaks belonged to the reduction of Co(IV)/Co(III), then to Co(II), as well as the reaction of Ni(III)/Ni(II) [58,59].

$$Ni(OH)_2 + OH^- \Leftrightarrow NiOOH + H_2O + e^- \quad (7)$$

$$Co_3O_4 + OH^- + H_2O \Leftrightarrow 3CoOOH + e^- \quad (8)$$

$$CoOOH + OH^- \Leftrightarrow CoO_2 + H_2O + e^- \quad (9)$$

Fig. 9 shows the influence of catalytic activity of the as-prepared Co_3O_4 nanostructures prepared by different C_2H_5OH/H_2O volume ratios for H_2O_2 electroreduction in 3.0 mol L^{-1} KOH + 0.5 mol L^{-1} H_2O_2. In order to better evaluate the catalytic performance of the as-prepared samples, we compared the current density of H_2O_2 reduction at unit mass on the five samples. As shown, the open circuit potential (OCP) of the five samples are closed to −0.15 V. In our previous work [60], we found that the OCP of H_2O_2 in acidic or alkaline electrolyte is actually a mixed potential of H_2O_2 electroreduction and electrooxidation simultaneously occurring at electrode surfaces and it is more close to the equilibrium potential of H_2O_2 electrooxidation rather than electroreduction. The introduction of ethanol as solvent obviously increased the catalytic performance. The sample of WE2 shows the best catalytic performance among the five samples, which is due to the ultra-fine Co_3O_4 nanowire net structure, enabling the fully exposure of active sites of catalyst to the electrolyte and providing a short diffusion path for both electrons and ions, thus leading to faster kinetics, lower

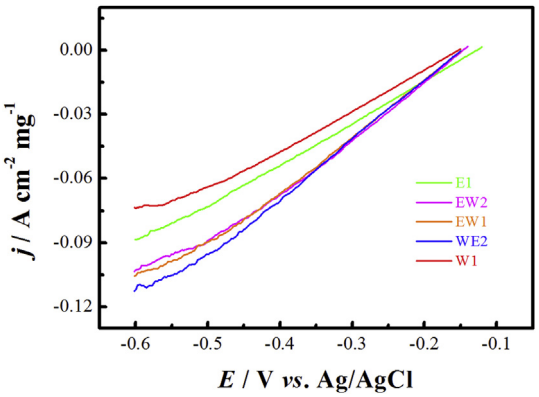

Fig. 9. The comparison of the as-prepared Co_3O_4 nanostructures in the growth solution with different C_2H_5OH/H_2O volume ratios (E1, EW2, EW1, WE2 and W1) for H_2O_2 reduction in 3.0 mol L^{-1} KOH + 0.5 mol L^{-1} H_2O_2. Scan rate: 10 mV s^{-1}.

overpotential and higher electrocatalytic reactivity. So we have chosen WE2 for a systematic study.

The dependence of H_2O_2 concentration for H_2O_2 electroreduction on the WE2 sample was shown in Fig. 10. The KOH concentration was kept at 3.0 mol L^{-1} with the various H_2O_2 concentrations from 0.0 mol L^{-1} to 0.6 mol L^{-1}. In order to eliminate the influence of the substrate, the Ni foam was also investigated in 3.0 mol L^{-1} KOH + 0.5 mol L^{-1} H_2O_2. As seen, the background signal caused by the Ni foam was almost none, indicating that the catalytic performance was caused by the Co_3O_4 grown on Ni foam substrate. The ultra-fine Co_3O_4 nanowire net exhibited an exciting catalytic performance for H_2O_2 electroreduction. It can be seen from Fig. 10 that there has no obvious reduction current on the as-prepared Co_3O_4 electrode without H_2O_2. After injection of H_2O_2 into the solution, the Co_3O_4 electrode responds quickly and H_2O_2 electroreduction reached to diffusion control when the H_2O_2 concentration is lower than 0.4 mol L^{-1}. The peak current density could reach to 60 mA cm^{-2} in the solution of 3.0 mol L^{-1} KOH+0.1 mol L^{-1} H_2O_2, and increased to 256 mA cm^{-2} with the increase of H_2O_2 concentration from 0.1 mol L^{-1} to 0.4 mol L^{-1}. So it is believed that the reduction current results from H_2O_2 electroreduction. High concentration of H_2O_2 did not improve the activity of H_2O_2 electroreduction at the as-formed Co_3O_4 electrode. In contrast, a further increase in the H_2O_2 concentration resulted in a decrease of current density, and gas bubbles were formed on the

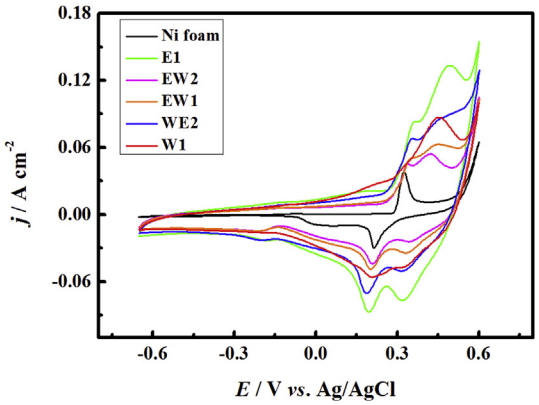

Fig. 8. Cyclic voltammograms of as-prepared Co_3O_4 nanostructures in the growth solution with different C_2H_5OH/H_2O volume ratios (E1, EW2, EW1, WE2 and W1) in 3.0 mol L^{-1} KOH. Scan rate: 50 mV s^{-1}.

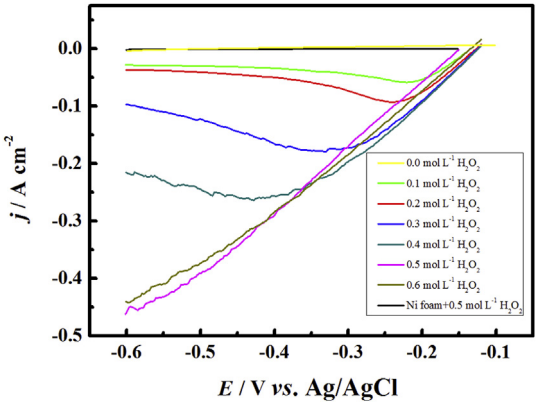

Fig. 10. The effect of H_2O_2 concentration for H_2O_2 reduction on the as-prepared Co_3O_4 using C_2H_5OH/H_2O volume ratio 1:2 (WE2) in 3.0 mol L^{-1} KOH + x mol L^{-1} H_2O_2 (x = 0.0–0.6). Scan rate: 10 mV s^{-1}.

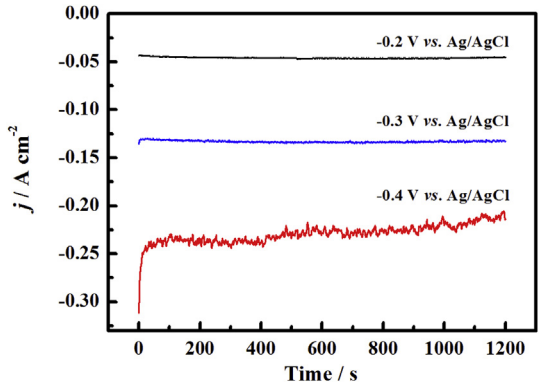

Fig. 11. Chronoamperometric curves for H_2O_2 reduction on the as-prepared Co_3O_4 using C_2H_5OH/H_2O volume ratio 1:2 (WE2) at different potentials in 3.0 mol L^{-1} KOH + 0.5 mol L^{-1} H_2O_2.

electrode surface by H_2O_2 hydrolysis, which blocked the H_2O_2 diffusion leading to the decrease in current density.

The electrochemical stability of ultra-fine Co_3O_4 nanowire net is measured by chronoamperometry (Fig. 11). The reduction currents reached a steady-state quickly after the potential was applied and slightly decreased within the test period at the three different potentials (−0.2 and −0.3 V), indicating that the ultra-fine Co_3O_4 nanowire net electrode has a good stability for catalyzing H_2O_2 electroreduction. However, at −0.4 V, the current decreases from 0.246 to 0.214 A cm^{-2} and the current fluctuation range also becomes wider, which may be that the high potentials produce even higher current densities, however, the hydrolysis of H_2O_2 becomes significant and the formation of oxygen gas bubbles on the electrode surface clearly occurred. The current density after 1200 s reaction at −0.2, −0.3 and −0.4 V were 0.045, 0.133 and 0.214 A cm^{-2}, respectively.

The comparison of H_2O_2 catalytic performance on ultra-fine Co_3O_4 nanowire net and other representative nanomaterials reported previously [19,58,61–64] were shown in Table 2. As shown in the result, our ultra-fine Co_3O_4 nanowire net displays excellent performance for H_2O_2 reduction than other metal oxides reported previously, almost comparable with the precious metals. These outstanding properties should be attributed to their structure and morphology that offer the following benefits: (1) the Co_3O_4 direct growth on the substrate may ensure the short transport path for electrons, leading to good conductivity; (2) the ultra-fine nanowire may also increase the electrode surface area, resulting in good mass transport. Due to the good electrons and ions transport, the H_2O_2 catalytic performance for ultra-fine Co_3O_4 nanowire net are remarkably improved.

Table 2
Comparison of H_2O_2 electroreduction on the ultra-fine Co_3O_4 nanowire net electrode and other representative nanomaterials reported previously.

Electrode	Performance[a] (A cm^{-2})	Ref.
Co_3O_4 nanowire/Ni foam[b]	0.125 (3 mol L^{-1} NaOH + 0.5 mol L^{-1} H_2O_2)	[19]
Co_3O_4 nanoparticle/Ni foam[c]	0.11 (3 mol L^{-1} NaOH + 0.6 mol L^{-1} H_2O_2)	[58]
Ag/Ni foam[b]	0.38 (3 mol L^{-1} NaOH + 0.5 mol L^{-1} H_2O_2)	[61]
CuO nanosheet/Cu foil[b]	0.007 (3 mol L^{-1} KOH + 0.5 mol L^{-1} H_2O_2)	[62]
Pd–Co_3O_4/Ti foil[b]	0.14 (3 mol L^{-1} KOH + 0.5 mol L^{-1} H_2O_2)	[63]
Fe–N–C/Ni foam[c]	0.07 (3 mol L^{-1} KOH + 0.6 mol L^{-1} H_2O_2)	[64]
Ultra-fine Co_3O_4 nanowire/Ni foam[b]	0.29 (3 mol L^{-1} KOH + 0.5 mol L^{-1} H_2O_2)	This work

[a] The current density of CV at −0.4 V (*vs.* Ag/AgCl, KCl).
[b] Nanomaterials direct growth on substrate.
[c] Nanopowder coated on substrate.

4. Conclusions

A facile synthesis of morphology-controlled Co_3O_4 nanostructures through the solvothermal synthesis was successfully demonstrated. With the control of the solvent composition, we have obtained five different nanostructures (nanosheet, nanowire, ultrafine nanowire net, nanobelts, and nano-honeycombs). The ethanol introduced in the synthesis processes plays an important role on the crystal size, morphology, as well as their catalytic performance for H_2O_2 electroreduction. The sample prepared in the 2:1 C_2H_5OH/H_2O solvent displays an ultra-fine nanowire net morphology, which possesses an open, porous nanostructure with a large surface area. These characteristics of Co_3O_4 nanostructures make it facilitate electrons/ions transferring and enhance the catalytic efficiency when used as an electrode. The resulting electrode shows better performance for H_2O_2 electroreduction in an alkaline medium in terms of the catalytic activity than Co_3O_4 nanowire array electrode prepared in the pure water solvent. In the solution of 3.0 mol L^{-1} KOH + 0.5 mol L^{-1} H_2O_2, the current density at −0.4 V could maintained at 0.214 A cm^{-2} during the test period. This simple solvothermal method has a great potential for the preparation of morphology-controlled Co_3O_4 nanostructures due to its facile synthesis, low cost, especially high performance for H_2O_2 reduction.

Acknowledgments

We gratefully acknowledge the financial support of this research by National Nature Science Foundation of China (21306033), the Fundamental Research Funds for the Central Universities (HEUCF20130910013) and Harbin Science and Technology Innovation Fund for Excellent Academic Leaders (2012RFXXG103).

References

[1] W. Sung, J.-W. Choi, J. Power Sources 172 (2007) 198–208.
[2] T. Bewer, T. Beckmann, H. Dohle, J. Mergel, D. Stolten, J. Power Sources 125 (2004) 1–9.
[3] F. Yang, K. Cheng, X. Liu, S. Chang, J. Yin, C. Du, L. Du, G. Wang, D. Cao, J. Power Sources 217 (2012) 569–573.
[4] F. Yang, K. Cheng, X. Xiao, J. Yin, G. Wang, D. Cao, J. Power Sources 245 (2014) 89–94.
[5] D. Cao, D. Chen, J. Lan, G. Wang, J. Power Sources 190 (2009) 346–350.
[6] R.K. Raman, S.K. Prashant, A.K. Shukla, J. Power Sources 162 (2006) 1073–1076.
[7] Ø. Hasvold, K.H. Johansen, O. Mollestad, S. Forseth, N. Størkersen, J. Power Sources 80 (1999) 254–260.
[8] R.R. Bessette, M.G. Medeiros, C.J. Patrissi, C.M. Deschenes, C.N. LaFratta, J. Power Sources 96 (2001) 240–244.
[9] B.H. Hong, S.C. Bae, C.-W. Lee, S. Jeong, K.S. Kim, Science 294 (2001) 348–351.
[10] A.I. Yanson, G.R. Bollinger, H.E. van den Brom, N. Agrait, J.M. van Ruitenbeek, Nature 395 (1998) 783–785.
[11] H. Han, T. Song, J.-Y. Bae, L.F. Nazar, H. Kim, U. Paik, Energy Environ. Sci. 4 (2011) 4532–4536.
[12] Y. Liang, C. Zhen, D. Zou, D. Xu, J. Am, Chem. Soc. 126 (2004) 16338–16339.
[13] D. Aili, F.-I. Tai, K. Enander, L. Baltzer, B. Liedberg, Angew. Chem. Int. Ed. 47 (2008) 5554–5556.
[14] M.-C. Daniel, D. Astruc, Chem. Rev. 104 (2003) 293–346.
[15] Y. Cui, Q. Wei, H. Park, C.M. Lieber, Science 293 (2001) 1289–1292.
[16] Z. Liu, R. Ma, M. Osada, N. Iyi, Y. Ebina, K. Takada, T. Sasaki, J. Am. Chem. Soc. 128 (2006) 4872–4880.
[17] M.D. Stoller, R.S. Ruoff, Energy Environ. Sci. 3 (2010) 1294–1301.
[18] G. Lota, K. Fic, E. Frackowiak, Energy Environ. Sci. 4 (2011) 1592–1605.
[19] G. Wang, D. Cao, C. Yin, Y. Gao, J. Yin, L. Cheng, Chem. Mater. 21 (2009) 5112–5118.
[20] Y. Gao, S. Chen, D. Cao, G. Wang, J. Yin, J. Power Sources 195 (2010) 1757–1760.
[21] L. Pan, H. Zhao, W. Shen, X. Dong, J. Xu, J. Mater. Chem. A 1 (2013) 7159–7166.
[22] B. Geng, F. Zhan, C. Fang, N. Yu, J. Mater. Chem. 18 (2008) 4977–4984.
[23] Y. Cui, Z. Wen, Y. Liu, Energy Environ. Sci. 4 (2011) 4727–4734.

[24] W. Li, G. Li, J. Sun, R. Zou, K. Xu, Y. Sun, Z. Chen, J. Yang, J. Hu, Nanoscale 5 (2013) 2901–2908.
[25] X. Wang, X.-L. Wu, Y.-G. Guo, Y. Zhong, X. Cao, Y. Ma, J. Yao, Adv. Funct. Mater. 20 (2010) 1680–1686.
[26] C.R. Sides, C.R. Martin, Adv. Mater. 17 (2005) 125–128.
[27] Y. Li, B. Tan, Y. Wu, Nano Lett. 8 (2007) 265–270.
[28] C.R. Sides, F. Croce, V.Y. Young, C.R. Martin, B. Scrosati, Electrochem. Solid-State Lett. 8 (2005) A484.
[29] C.J. Patrissi, C.R. Martin, J. Electrochem. Soc. 148 (2001) A1247.
[30] G.-Y. Zhao, C.-L. Xu, D.-J. Guo, H. Li, H.-L. Li, J. Power Sources 162 (2006) 492–496.
[31] L. Liu, E. Pippel, R. Scholz, U. Gösele, Nano Lett. 9 (2009) 4352–4358.
[32] D. Huesmann, P.M. DiCarmine, D.S. Seferos, J. Mater. Chem. 21 (2011) 408–413.
[33] Y. Liu, J. Goebl, Y. Yin, Chem. Soc. Rev. 42 (2013) 2610–2653.
[34] X.-M. Chen, M.-L. Tong, Acc. Chem. Res. 40 (2006) 162–170.
[35] X.-M. Zhang, Coord. Chem. Rev. 249 (2005) 1201–1219.
[36] B.L. Cushing, V.L. Kolesnichenko, C.J. O'Connor, Chem. Rev. 104 (2004) 3893–3946.
[37] L.-X. Yang, Y.-J. Zhu, L. Li, L. Zhang, H. Tong, W.-W. Wang, G.-F. Cheng, J.-F. Zhu, Eur. J. Inorg. Chem. 2006 (2006) 4787–4792.
[38] H.-P. Cong, S.-H. Yu, Cryst. Growth Des. 9 (2008) 210–217.
[39] D. Wang, Q. Wang, T. Wang, Inorg. Chem. 50 (2011) 6482–6492.
[40] Z.W. Zhao, Z.P. Guo, H.K. Liu, J. Power Sources 147 (2005) 264–268.
[41] X. Li, C. Tang, M. Ai, L. Dong, Z. Xu, Chem. Mater. 22 (2010) 4879–4889.
[42] I. ul Haq, K. Akhtar, Chem. Mater. 9 (1997) 2659–2665.
[43] X. Jing, S. Song, J. Wang, L. Ge, S. Jamil, Q. Liu, T. Mann, Y. He, M. Zhang, H. Wei, L. Liu, Powder Technol. 217 (2012) 624–628.
[44] S. Todorova, A. Naydenov, H. Kolev, J.P. Holgado, G. Ivanov, G. Kadinov, A. Caballero, Appl. Catal. A 413–414 (2012) 43–51.
[45] Z. Yu, S.S.C. Chuang, J. Catal. 246 (2007) 118–126.
[46] S. Burikov, T. Dolenko, S. Patsaeva, Y. Starokurov, V. Yuzhakov, Mol. Phys. 108 (2010) 2427–2436.
[47] M.P. Luda, L. Costa, P. Bracco, S.V. Levchik, Polym. Degrad. Stab. 86 (2004) 43–50.
[48] C. Ehrhardt, M. Gjikaj, W. Brockner, Thermochim. Acta 432 (2005) 36–40.
[49] K.T. Ehlsissen, A. Delahaye-Vidal, P. Genin, M. Figlarz, P. Willmann, J. Mater. Chem. 3 (1993) 883–888.
[50] M.Y. Nassar, Mater. Lett. 94 (2013) 112–115.
[51] H. Lewandowski, E. Koglin, R.J. Meier, Vib. Spectrosc. 39 (2005) 15–22.
[52] H.T. Flakus, B. Hachuła, Vib. Spectrosc. 56 (2011) 170–176.
[53] E. Kukulska-Zając, K. Góra-Marek, J. Datka, Microporous Mesoporous Mater. 96 (2006) 216–221.
[54] Y. Wang, H. Xia, L. Lu, J. Lin, ACS Nano 4 (2010) 1425–1432.
[55] J. Jiang, J.P. Liu, X.T. Huang, Y.Y. Li, R.M. Ding, X.X. Ji, Y.Y. Hu, Q.B. Chi, Z.H. Zhu, Cryst. Growth Des. 10 (2009) 70–75.
[56] S. Kunjara Na Ayudhya, P. Tonto, O. Mekasuwandumrong, V. Pavarajarn, P. Praserthdam, Cryst. Growth Des. 6 (2006) 2446–2450.
[57] X.H. Xia, J.P. Tu, Y.Q. Zhang, Y.J. Mai, X.L. Wang, C.D. Gu, X.B. Zhao, J. Phys. Chem. C 115 (2011) 22662–22668.
[58] D. Cao, J. Chao, L. Sun, G. Wang, J. Power Sources 179 (2008) 87–91.
[59] A.E. Sanli, A. Aytaç, Int. J. Hydrogen Energy 36 (2011) 869–875.
[60] X. Jing, D. Cao, Y. Liu, G. Wang, J. Yin, Q. Wen, Y. Gao, J. Electroanal. Chem. 658 (2011) 46–51.
[61] W. Yang, S. Yang, W. Sun, G. Sun, Q. Xin, J. Power Sources 160 (2006) 1420–1424.
[62] Y. Li, D. Cao, Y. Liu, R. Liu, F. Yang, J. Yin, G. Wang, Int. J. Hydrogen Energy 37 (2012) 13611–13615.
[63] K. Cheng, F. Yang, Y. Xu, L. Cheng, Y. Bao, D. Cao, G. Wang, J. Power Sources 240 (2013) 442–447.
[64] Y. Tian, J. Huang, Y. Gao, D. Cao, G. Wang, J. Solid State Electrochem. 16 (2012) 1901–1906.